Journal of NAMP 72, (2026) 81-102

The Nigerian Association of Mathematical Physics

Journal homepage: https://nampjournals.org.ng

IMPACTS OF EULER DECONVOLUTION ON POTENTIAL FIELD GRADIENTS: IMPLICATIONS ON STRUCTURAL EVALUATION OF HIGH RESOLUTION AEROMAGNETIC DATA OF ILORIN (SHEET 223) NORTH-CENTRAL NIGERIA

Ishola S. A.

Department of Earth Sciences, Olabisi Onabanjo University Ago-Iwoye, P.M.B 2002, Ago-Iwoye, Ogun State, Nigeria.

ARTICLE INFO

Article history:
Received xxxxx
Revised xxxxx
Accepted xxxxx
Available online xxxxx

Keywords:
Euler deconvolution,
Analytic signal,
Field gradient,
Derivatives,
Noise.

ABSTRACT

This study presents a quantitative interpretation of high-resolution aeromagnetic data over Ilorin and its environs (sheet 223), North-Central Nigeria. The data, sourced from the Nigerian Geological Survey Agency (NGSA), processed using Geosoft Oasis Montaj™ 8.4v, and were analyzed to delineate subsurface structural features and lithological variations for geological mapping and mineral exploration. The computational techniques of field gradients in a clean pattern were highlighted alongside with the suggested new technique for rejecting invalid Euler solutions while the modified Euler deconvolution algorithm was equally demonstrated exemplifying it on synthetic models as well as on Ilorin and its environs. The analytical signal revealed a value range of 0.0002 to 3.4127 nT/m while the 3D Euler Deconvolution revealed depth values ranging from 95m to 292m; depth estimation and geometry of magnetic sources. The integration of quantitative outputs indicates that the area is structurally complex, with multiple fractures, faults and lithological boundaries concealed beneath the surface..

1. INTRODUCTION

The measurements of gradient or total magnetic field are geophysically acquired from the earth, either in the air, or on the ocean covering a large expanse of scales and for a diverse variety of environmental tasks. Therefore, expanded from the initial application principally as a significant device for exploration of iron ore and overall investigation for minerals [1-2], hydrocarbon explorations [3], groundwater investigation [4], archeological ruins [5-6] environmental contamination issues [7], geothermal resource studies [8] and complex fault system [9-14]. In areas of where geological formations conveying a magnetic signature dip at a notable angle, a magnetic survey can be undertaken to effectively and precisely map the subsurface geology [5, 15]. For both regional and detailed exploration studies, magnetic measurements are highly significant for unravelling the regional tectonic setting.

*Corresponding author: ISHOLA, S. A.
E-mail address: ishola.sakirudeen@oouagoiwoye.edu.ng
https://doi.org/10.60787/jnamp.vol72no.662

For instance, faults and other structural terrain boundaries are frequently acknowledged by the notable contrast in magnetic fabric across the line of contact [15]. Also, the structural study of tectonic setting is a significant economic implication of magnetic surveys particularly in a large hydrocarbon and geothermal explorations as well as in geotechnical cum foundation engineering investigations. Besides, for the most part, several published reports have typically revealed that basin fill possesses a much lower susceptibility than the crystalline basement. Therefore, it is highly possible to grant a common estimation of the depth to basement information and over favourable circumstances, quantitative mapping of basement structures such as faults and horst blocks are readily provided [16]. The incidences of magnetic anomalies are attributed to simple geophysical models such as dykes and faults and the model parameters are usually determined through a well-designed inversion scheme. Fast processing and consequent speedy interpretation of such simple geometric models is often undertaken through graphical approaches with characteristic curves included [17]; although rigorous analyses of the acquired data are often involved via varying inversion schemes on computers thereby harnessing various optimization techniques [18-22]. A significant view of the interpretation of magnetic data is the issue of location determination as well as the type of the magnetic source. This primary objective has become particularly significant recently due to the expanding volume of magnetic data that are acquired for diverse studies particularly for environmental, archeological and geological applications. For the sake of this objective, a variety of mathematical derivations centered on the employment of derivatives of the magnetic field applications and image processing techniques have been established to determine magnetic source parameters encompassing locations of boundaries as well as depths. The detail investigation of these studies has been undertaken by [5]. In this study Euler deconvolution, analytical signal and gradient methods were utilized. Euler deconvolution and the analytical signal are geophysical interpretation techniques used with aeromagnetic data to estimate the depth of magnetic sources, such as the basement rocks, and to characterize geological structures like faults, contacts, and intrusions. Euler deconvolution provides depth estimates by applying Euler's homogeneity equation and requires a structural index related to the source geometry. The analytical signal, on the other hand is an operation that effectively removes the background field, allowing for both location and depth determination without needing to know the structural index beforehand [26].

The purpose of Euler deconvolution is to semi-automatically determine the location and depth of geological structures including the basement [27-31]. Euler deconvolution utilizes Euler's homogeneity equation which relates the potential field (magnetic or gravity) to location of its sources and the degree of homogeneity (structural index) [32]; the quality of the depth estimation depends on selecting the correct structural index which represents the geometry of the causative bodies [26-27, 31]. It's area of applied for delineating contacts between sedimentary layers and basement rocks, estimating depths to sources like dykes, faults, and intrusions [27-31]. The purpose of analytical signal is to enhance anomalies and, by removing the background field, to provide a model-independent tool for source location and depth determination. It is a mathematical transformation of the magnetic field that helps to remove the influence of the background regional field [27, 30]. The analytical signal allows for the solution of both the source location and structural index from the same data because it eliminates the background field making it a powerful interpretive tool. Analytical signal is primarily used in conjunction with Euler deconvolution to improve the accuracy of source parameter estimates and to delineate complex geological boundaries [32]. Euler deconvolution and analytical signal are highly significant in aeromagnetic data interpretation in different ways; the contributions of both methods enhance the understanding of the depth to the magnetic basement which is crucial for resource exploration (minerals, hydrocarbons) and geological mapping; they help in the characterization of geological structures

by identifying and mapping linear features such as faults, folds, and shear zones as well as contacts and intrusions, providing insight into the subsurface architecture [32]; it serves as a semi-automatic technique making the interpretation of large aeromagnetic datasets more efficient and rapid compared to manual methods [33]; the analytical signal can improve the quality of data input for Euler deconvolution, leading to more reliable depth estimations and better characterization of geological features [34-36].

The aeromagnetic method of geophysical investigation using Euler deconvolution and analytical signal technique is highly necessary and beneficial for basement depth investigation in Ilorin to identify subsurface geological structures like dykes, determine depth and thickness of sedimentary basins, and map mineralization zones for resource exploration and infrastructural planning. This method provides a cost effective, large scale, non-invasive overview of the subsurface, crucial for understanding the area's complex Precambrian basement complex geology which has implications for groundwater potential, geothermal resources and engineering stability [37]. The method effectively identifies linear features such as faults, joints, and dykes which are zones of weakness in the subsurface that can influence groundwater flow and structural stability; it helps in ascertaining the depth to the magnetic basement and map the thickness of overlying sedimentary layers which is vital for understanding subsurface topography and potential resource locations [38-40]; by mapping magnetic source bodies and identifying mineralization zones, the method aids in discovering potential solid mineral deposits within the basement complex [41]; the depth o basement and structural features identified through aeromagnetic surveys are crucial for evaluating groundwater potential and identifying areas suitable for geothermal exploitation [38, 42-43]; understanding the depth to basement and the distribution of subsurface structures is essential for selecting stable sites and avoiding risk-prone zones during infrastructure planning and development. [44-46]. Necessity of the study for basement depth investigation in Ilorin cannot be overemphasized. The Ilorin area is situated within the Precambrian basement complex which has undergone intense deformation through observed multiple phases of faulting and folding within the Pan-African Orogenic episodes. Investigating the basement's depth and structure is thereby essential for effective characterizations of these complex geological formations [47]; the study area has potential for both solid mineral deposits and groundwater, requiring detailed subsurface mapping to locate and assess these resources effectively; a comprehensive understanding of the basement depth provides foundational information for broader regional geological mapping and analysis, linking the Ilorin area to larger tectonic framework [49]; aeromagnetic surveys are a non-invasive, reconnaissance level technique that provides a broad-scale view of the subsurface, making it an efficient and cost-effective initial step before more detailed and expensive geophysical investigations are employed [50-65].

Study Area

Topographic and climate description of Ilorin

The investigated area is well drained by various streams and their connecting tributaries. The tributaries often display a dendritic drainage pattern. The major rivers are Asa and Agba Rivers, while minor oners include Oyun and Aluko Rivers. The terrain is highly undulating and very much dissected by incursion of interfering rivers and streams. The highest recorded altitude is about 1200m above the mean sea level corresponding to the peak of Sobi Hill (migmatite), while along major streams the altitude is about 250m above the mean sea level (Abolarin and Ibrahim, 2015). The study lies within the Guinea savannah ruminant tropical forest with two distinct seasons; rainy and dry season. The rainy season often begins around March and completes seasonal functions in October with annual average rainfall of 1200mm. The dry season commences in November and wrap-up its activities in March. The humidity ranges between 60% and 89% and mean annual

temperature is between 27 and 30°C [66]. Ilorin has a typical tropical savannah climate with a wet season from April to October and a dry season from November to April. The annual rainfall ranges from 990.3 to 1318 mm [67-68]. The maximum temperatures range from 33 to 37 °C with March being the hottest month. The relative humidity varies and impurities and humidity have increased between 1978 and 2017 [69]. Ilorin experiences the urban heat island effect with higher temperatures in the urban centre compared to surrounding areas due to land cover and other factors [67]. Ilorin has a dissected topography (Figure 1) located in North-central Nigeria and is situated in a transition zone between rainforest and Guinea Savannah, experiencing distinct wet and dry seasons. The city's topography is characterized by varying elevations with higher elevations in the northern parts and a higher concentration of settlements in the Southern region. Ilorin also lies near the Awun river, a minor tributary of the Niger river [67].

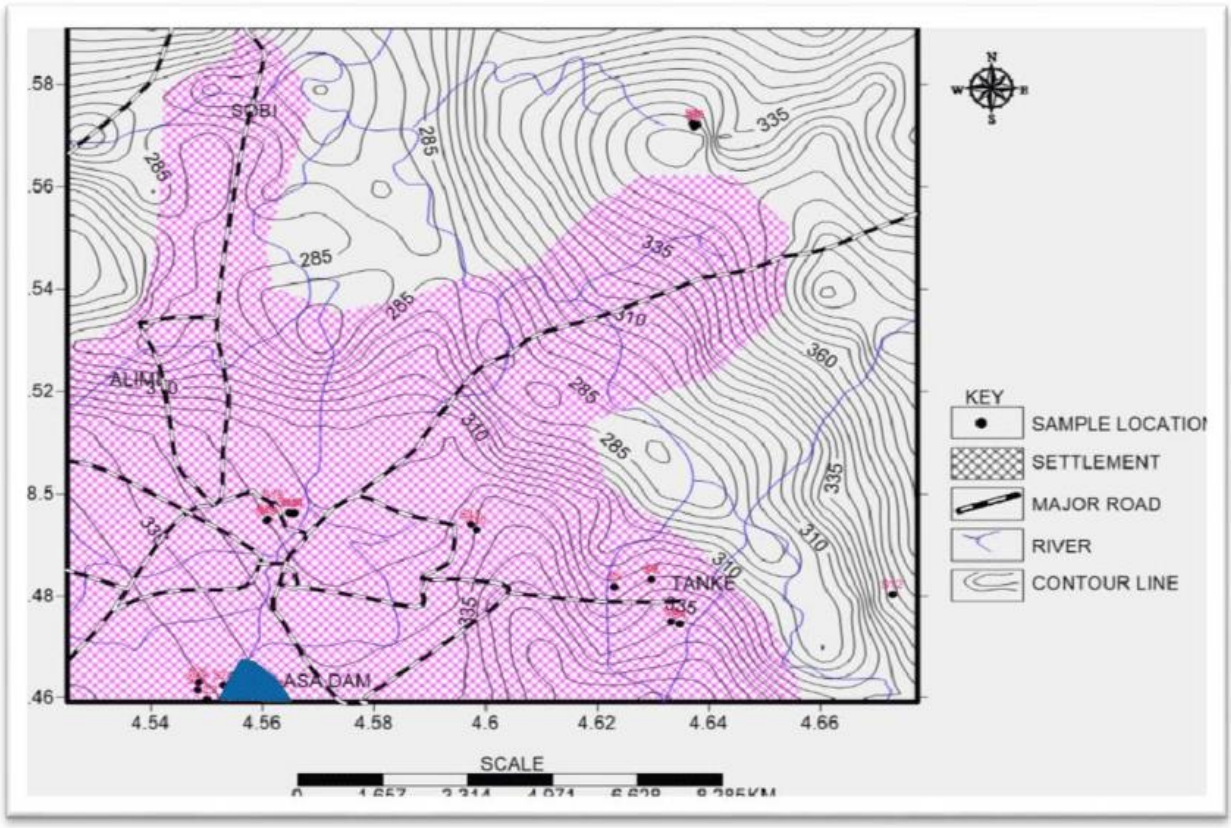

Figure 1: Topographic Map of the study area [68]

Physiography and Geology of the study area

The study area (Ilorin Sheet 223) is bounded by Longitude 4°30"E and Longitude 5°00"E; and Latitude 8°00"N and Latitude 8°30"N covering an approximate area of 2,601km². The study area is part of Nigeria's basement Complex terrain. The age of the rocks is estimated to be Precambrian, with a principal occurrence of Biotite granite-Migmatite-Gneiss-Quartzite complex and Schist belt as the major geological compositions which are adjacent to each other [70]. Ilorin town is situated on the undifferentiated Precambrian basement complex rocks that are granitic and metamorphic in origin. These rocks are good representation of the deeper, fractured aquifer which is overlain partly by a shallow and porous aquifer within the lateritic soil cover [71]. The formed rock units are integral part of the regional Southwestern highlands of Nigeria that runs from NW to SE on a

parallel line to the river Niger [72-73]. Fractured zones trending SW-NE are present and can act as weak zones for groundwater potentials.

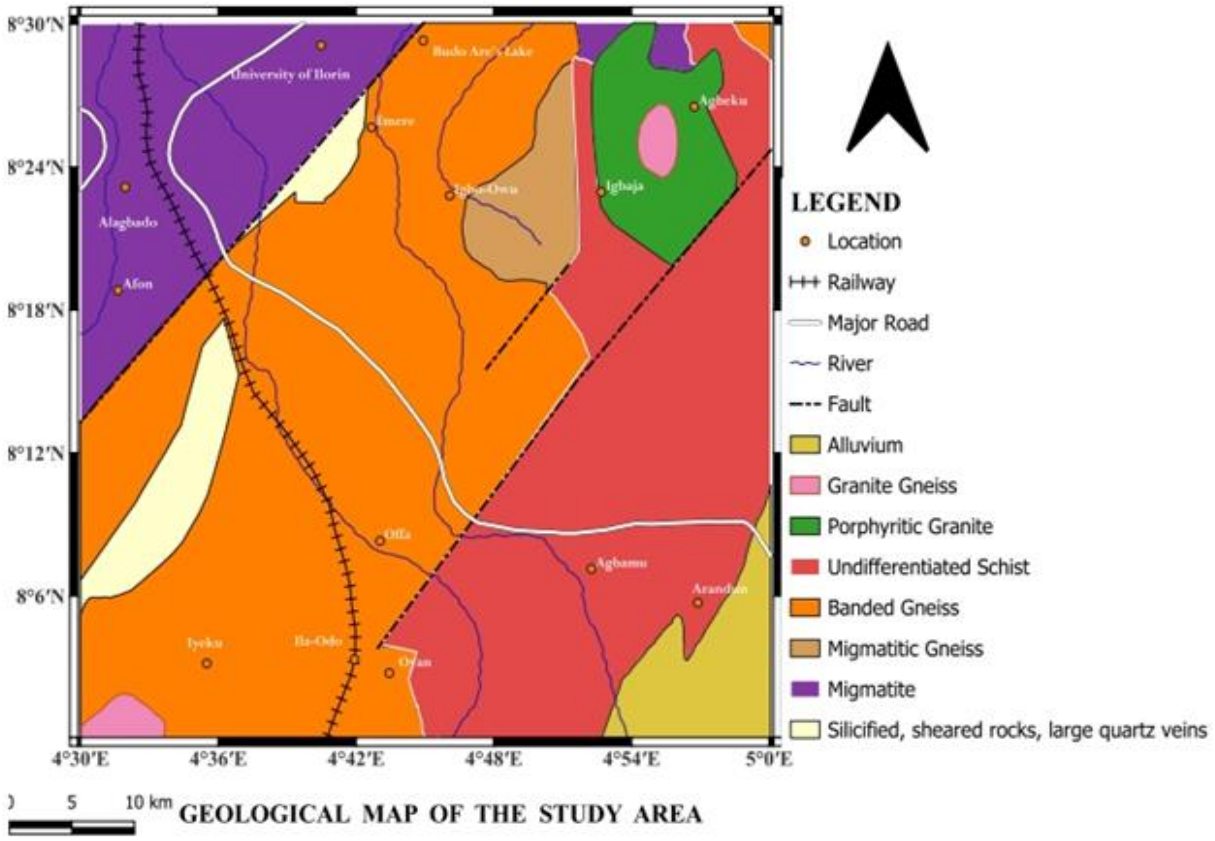

Figure 2: Geological Map of the Study Area [74]

MATERIALS AND METHODS

Theoretical Background

Integration of Euler Deconvolution Technique to Potential Field Gradients

Different solid and ore mineral exploration projects undertakings are often accompanied with the gathering of large volumes of aeromagnetic field data which more often than not require further technical interpretation. Diverse semi-automatic interpretation techniques in existence such as Werner deconvolution [75], Source parameter imaging and Euler deconvolution [76-77] have always being sources of assistance to the interpreter. These techniques utilize different physical models and consequently produce different outputs, but in the long-run, the task of obtaining source depth and location estimates will be accomplished. Some other techniques also provide the dip and susceptibility of certain kinds of source models [77]

The principal function of Euler deconvolution is to model the subsurface of a geological structure as a set of simple sources such as monopoles and dipoles which are characterized by structural index often denoted with *SI*; this can be used to estimate the depth and location of potential field sources of a given structural index. Deterministic values of the structural index are 3 and 2 respectively illustrated for a dipole and a point mass condition. The two-dimensional form of Euler deconvolution for a homogeneous anomaly field denoted as h measured at a specified location (p, r) is presented in equation 1 as

$$\frac{\partial h}{\partial p}(p - p_0) + \frac{\partial h}{\partial r}(r - r_0) = -SI.h \qquad (1)$$

where p_0 and r_0 are respectively source location and depth [76, 78]

Integration of Euler Deconvolution to Vertical and Horizontal Gradients

There is a provision of an improved source resolution when Euler deconvolution is applied to the vertical gradient of either gravity or magnetic field such that

$$\frac{\partial}{\partial p}\left(\frac{\partial^t h}{\partial r^t}\right)(p - p_0) + \frac{\partial}{\partial r}\left(\frac{\partial^t h}{\partial r^t}\right)(r - r_0) = -(SI + t)\left(\frac{\partial^t h}{\partial r^t}\right) \qquad (2)$$

where *t* is the order of the gradient used which may not necessarily be an integer [27, 79-83]. Similarly, the same conceptual model can be applied to the horizontal gradient as illustrated in equation 3 [83-84].

$$\frac{\partial}{\partial p}\left(\frac{\partial^t h}{\partial p^t}\right)(p - p_0) + \frac{\partial}{\partial r}\left(\frac{\partial^t h}{\partial r^t}\right)(r - r_0) = -(SI + t)\left(\frac{\partial^t h}{\partial p}\right) \qquad (3)$$

Solutions from the derivative data have the capacity to group over the body corners much more accurately than those obtained from the total field. It is worthy of notes that when utilizing a derivative of order t, the structural index used is increased by t. This enhances the reduction of the sensitivity of the solutions to the structural index utilized because if the structural index is altered by a given proportion of change, Δ, the fractional alteration in the effective structural index would be $\Delta/_{SI}$ if the total magnetic field is adopted but if the order of *t* derivative is adopted, the fractional change in the effective structural index would be $\Delta/_{(SI+t)}$. One notable factor responsible for the horizontal derivative of the observed field to exhibit an improved state in the Euler solutions in comparison to those that are derived from total magnetic field implies that the resultant differentiation exhibited on the asymmetrical magnetic anomalies can rework them to be more symmetrical [83-84]. [85] applied Euler deconvolution technique to measured gravity tensor data and finally discovered that that it actually improved the performance of the gravity method. The main focus on this study is magnetic rather than gravity data and tensors were no even utilized because field measured gravity tensor data somewhat scarce and expensive to come by compared to aeromagnetic field data.

The integration of Euler deconvolution simultaneously to the lateral and vertical derivatives on the field can be undertaken using several means. First and foremost, equation 2 and 3 can be simplified simultaneously to yield equation 4 as presented below.

$$\begin{bmatrix} \frac{\partial}{\partial p}\left(\frac{\partial^t h}{\partial p^t}\right) \\ \frac{\partial}{\partial p}\left(\frac{\partial^t h}{\partial r^t}\right) \end{bmatrix}(p - p_0) + \begin{bmatrix} \frac{\partial}{\partial r}\left(\frac{\partial^t h}{\partial p^t}\right) \\ \frac{\partial}{\partial r}\left(\frac{\partial^t h}{\partial r^t}\right) \end{bmatrix}(r - r_0) = -(SI + t)\begin{bmatrix} \left(\frac{\partial^t h}{\partial p^t}\right) \\ \left(\frac{\partial^t h}{\partial r^t}\right) \end{bmatrix} \qquad (4)$$

Also, addition or subtraction may be alternatively applied on equation 2 and 3 and consequently expressed as equation 5

$$\left(\frac{\partial^{t+1} h}{\partial p^{t+1}} \pm \frac{\partial}{\partial p}\left(\frac{\partial^t h}{\partial r^t}\right)\right)(p - p_0) + \left(\frac{\partial}{\partial r}\left(\frac{\partial^t h}{\partial p^t}\right) \pm \frac{\partial^{t+1} h}{\partial r^{t+1}}\right)(r - r_0) = -(SI + t)\left(\frac{\partial^t h}{\partial p^t} \pm \frac{\partial^t h}{\partial r^t}\right) \qquad (5)$$

It can be observed from equation 5 that the latter form of the equation involved the subtraction of the derivatives of the field which naturally makes it susceptible to noise challenges. Also, both of

the last equations (equation 4 and 5) were however recognized to be robust with respect to noise particularly when the noise is emanating from the uncorrelated horizontal and vertical gradients. This observed robustness therefore permits the integration of higher order derivatives, thereby projecting more accurate and precise source locations [84]. According to that deliberately chose an order of derivative sufficiently high to produce noise problems in different source models contacts and fault models inclusive; despite adopting order of 2.75 horizontal and vertical derivatives, the resultant effects of the computation reveals that the Euler solutions from all the different approaches were found clustering over the contact with those of equation 5 being located as the most accurate with similar output being recorded for a fault model. Hence, it was concluded that though, higher order derivatives improve the resolution of the Euler solutions, the noise problems generated from the processing are often displayed in a contrary manner for the degradation of the resolution [84].

Impacts of Euler Deconvolution on Analytical Signal

[15] introduced the concept of the analytic signal for magnetic interpretation and revealed that its amplitude yields a bell-shaped function over each corner of a 2D body with polygonal cross-section. When it is an isolated corner, the maximum deflection of the bell-shaped curve is locally positioned at the exact spot over the corner and the width of the displayed curve exhibited a localized position at half its maximum amplitude being equal to twice the depth to the corner. The determination of these aforementioned parameters may not be affected by the availability of remnant magnetization. Horizontal locations are usually appropriately determined by this method, but the actual depth determinations are only recognizable for polyhedral bodies [5]. The 3D analytical signal amplitude emanating from a total magnetic intensity (TMI) map was introduced by [23] is has since been expansively utilized in magnetic interpretation [5].

An Analytical signal can be produced from the gradients of the potential field as presented in equation (6) and is amplitude presented in equation (7) [84].

where Analytical signal is denoted as *AS*.

$$AS(p, r) = \frac{\partial h}{dp} + i\frac{\partial h}{dr} \quad (6)$$

$$|AS(p,r)| = \sqrt{\left(\frac{\partial h}{dp}\right)^2 + \left(\frac{\partial h}{dr}\right)^2} \quad (7)$$

[84] suggested the integration of Euler deconvolution to analytical signal, $|AS(p,r)|$, after the accomplishment of this, the structural index must therefore be increased by 1 in comparison to the chosen value used for the total magnetic field.

Integration of Euler Deconvolution on Simple Model Analytical Signal (SMAS) and Complex Model Analytical Signal (CMAS)

[84-86] and [87] while at different times exploited the properties of the observed analytical signal models for the primary purpose of deriving field information on source geometry and depth using the analytic signal amplitude in a singular fashion. Euler deconvolution can also be employed to the complex analytic signal function $|AS(p,r)|$ itself when the structural index is again increased by 1. This can be analytically proven for gravity anomaly from a point source as a case study as shown below from equation (8) to (15).

From a point source, the gravity anomaly is presented as

$$g = \frac{BKr}{(p^2 + r^2)^{\frac{3}{2}}} \quad (8)$$

where B mathematically represents the universal gravitational constant, K represents the body mass and p and r respectively represents the source locations and depth in Cartesian coordinates

$$\frac{\partial g}{\partial p} = \frac{-3BKrp}{(p^2 + r^2)^{\frac{5}{2}}} \quad (9)$$

$$\frac{\partial g}{\partial z} = \frac{BK}{(p^2 + r^2)^{\frac{3}{2}}} - \frac{3BKr^2}{(p^2 + r^2)^{\frac{5}{2}}} \quad (10)$$

when equation (10) is inserted into equation (6), the analytic signal response is produced for the point source and if this is further differentiated with respect to both p and r and consequently inserted into equation (1), produces equation 11.

$$BKp\left[\frac{(12p^2r - 3r^3) + i\ (12pr^2 - 3p^3)}{(p^2 + r^2)^{\frac{7}{2}}}\right] + BKr\left[\frac{(-3p^3r + 12pr^3) + i(-9r^2p^2 + 6r^4)}{(p^2 + r^2)^{\frac{7}{2}}}\right] =$$

$$-(SI + 1)\left[\frac{-3BKrp}{(p^2 + r^2)^{\frac{5}{2}}} + i\left(\frac{BK}{(p^2 + r^2)^{\frac{3}{2}}} - \frac{3BKr^2}{(p^2 + r^2)^{\frac{5}{2}}}\right)\right] \quad (11)$$

Further mathematical simplifications of equation (11) produces equation (12) such that

$$\left[\frac{(12p^2r - 3pr^3 - 3p^3r^2 + 12pr^4) + i\,(-3p^4 + 12p^2r^2 - 9p^2r^3 + 6r^5)}{(p^2 + r^2)^{\frac{7}{2}}}\right] =$$

$$-(SI + 1)\left\{\left[\frac{-3rp}{(p^2 + r^2)^{\frac{5}{2}}} + i\left(\frac{1}{(p^2 + r^2)^{\frac{3}{2}}} - \frac{3r^2}{(p^2 + r^2)^{\frac{5}{2}}}\right)\right]\right\} \quad (12)$$

$$= -(SI + 1)\left[\frac{-3rp + i(p^2 - 2r^2)}{(p^2 + r^2)}\right] \quad (13)$$

Therefore, equation 13 is a proof that the equation of Euler deconvolution holds for the Complex Valued Analytical Signal of the Gravitational Anomaly from a point source such that when SI = 2 and 3 equations (14) and (15) will be respectively produced.

$$= \left[\frac{9pr + i(-3p^2 + 6r^2)}{(p^2 + r^2)}\right] \quad (14)$$

$$= \left[\frac{12pr + i(-4p^2 + 8r^2)}{(p^2 + r^2)}\right] \quad (15)$$

The 3D analytical signal amplitude of a total magnetic intensity serves as interpretive technique as a means of positioning anomalies directly above or over their magnetic sources. The analytic signal of a magnetic field intensity anomaly has been empirically defined in 3D as

$$|AS(p, q, r)| = \frac{\partial I}{\partial p}\,\hat{p} + \frac{\partial I}{\partial q}\,\hat{q} + j\,\frac{\partial I}{\partial r}\,\hat{r} \quad (16)$$

Where I is the magnetic intensity, $j\sqrt{-1}$ and *p, q* and *r* are unit vectors as emplaced in a Cartesian coordinate system [5, 23]. The outputs are however strongly dependent on the directional line of magnetization which are conspicuously in sharp contrast with the 2D [5, 88]. The observed steepest horizontal gradient of a potential field anomaly tends to overlie the edges of the source body. Indeed, the steepest gradient is technically expected to be located directly over the edge of the body on the limiting conditions that the delineated edge is vertical and are far separated from all other edges or sources [5, 88]. The horizontal gradient tends to possess maxima exhibition locally positioned over edges of magnetic or gravity sources. When this is integrated into two dimensional surveys, the horizontal gradient tends to reorganize narrow ridges over abrupt alteration in observed magnetization or density. The possible Location of maxima deflection in the horizontal gradient can be undertaken by simple inspection but [85] largely automation of the procedure with an algorithm that scans the rows and columns of gridded data and records the locations of maxima in a file for future analysis and plotting. The Interpretation of the horizontal gradient in terms of density or magnetization contrasts, and ultimately with regards to subsurface geology requires several underlying assumptions. In particular, it is assumed that the occurrence of the observed contrasts in physical proportions is located across the vertical and abrupt boundaries isolated from other sources.

Though, [89] provided an interpretation method based on the wave numbers derived from the analytic signal of the field data, still, the approaches utilized did not involve Euler deconvolution. The integration of Euler deconvolution to the first vertical derivative of $|AS(p,r)|$ using structural index increased by 2 produced noticeably improved outputs compared to the application to just $|AS(p,r)|$. However, its computations involved 3rd order derivatives and problems with noise were common when such higher order derivatives were used when working with measured field data.

Computation of Field Gradients

Field gradient refers to variation of magnetic field with spatial position typically described in three principal axes (G_p, G_q and G_z) which is generated by a set of gradient coils. This variation causes nuclei at different positions to experience slightly different magnetic field leading to distinct processional frequencies that can be utilized to allocate spatial information for image reconstruction.

Computation of vertical gradients in a clean pattern

Vertical gradients are computed in a clean manner such that any noise present in the data can be set on amplification when its gradients are computed since gradient filters are noted as high pass filters; field gradients of order greater than one are utilized in equation (2) and (5). When gradients are calculated in the frequency domain, they seem to exhibit higher noise levels than those that are calculated in the space domain due to the resultant practical problems associated with the implementation of the Fourier transform like data stationarity and edge effects. Notwithstanding, all hands must be on the desk to compute the gradient in a manner that is as noise-free as possible otherwise, the output of Euler deconvolution solutions would be adversely hampered. Though the direct computation of space domain of vertical gradients is impractical, there are existing techniques that can be adopted to reduce to one degree. These techniques exploit the fact that horizontal derivatives are simple to calculate in the space domain while the vertical derivatives can be calculated from the horizontal derivatives in various means [84]. A Hilbert transform pair is formed from the first horizontal derivative and first vertical derivatives [85]. Therefore, when a Hilbert transform is applied in the frequency domain, the first vertical derivative can be calculated from the first horizontal derivative mathematically derived from the space domain. This could just

be a mere rotation of datasets because it does not change the content embedded in the frequency. The second vertical derivative can equally be derived from the second horizontal derivative using Laplace's equation as observed in equation 17 [84-85, 90]

$$\nabla^2 h = \frac{\partial^2 h}{\partial p^2} + \frac{\partial^2 h}{\partial q^2} + \frac{\partial^2 h}{\partial r^2} \quad (17)$$

In order to permit the stable calculation of vertical gradients of any order of integers, the generalized approach of [91] was utilized. There are three (3) distinct stages embedded in this concept. First and foremost, the vertical integral of the data is calculated. This is followed by the calculation of the second horizontal derivatives of the vertical integral in the space domain, and the derivation of the required vertical derivative from Laplace's equation. This aforementioned procedure can further be enhanced to also obtain vertical gradients of fractional order. For instance, if the vertical derivatives of order 1.75 was needed, the second horizontal derivatives of the vertical integral of order −0.25 would in turn be calculated, the output emanating from this processing would then be used to produce the vertical derivative of the required order of 1.75 using the Laplace's equation in equation 17.

Though, the integer order of the horizontal gradients are quite simple to calculate in the space domain, greater efforts are required for the calculation of fractional order of clean field gradient. Also, despite the fact that fractional order of horizontal derivatives is computed in the space domain, several hundred coefficients are needed by the filters for the accomplishment of reasonable accuracy, making them redundant in practical sense. The modification of the adopted Fedi and Florio's approach utilizing the generated algorithm for the computation of integer order of vertical gradients was found to be reliable in addressing the problem [91] [84, 92]. To obtain a horizontal gradient aligning itself to the fractional order *a*, first requires the integration of the data by *b-a* where *b* is the subsequent integer value greater than *a.* the b^{th} horizontal gradient of the output can then be computed in the space domain. For instance, to obtain the horizontal gradient of order 0.75, the data is first integrated by order −0.25 ($\approx -33\%$) in the frequency domain, then differentiated by order 1 ($\approx 133\%$) in the space domain. It is quite worthy of note that this approach is computationally not much slower when placed side by side in comparison with the standard frequency domain operations due to the rapid processing of the space domain computations [84]

Position of invalid Euler solutions

Large numbers of invalid solutions are generated as consequents of reasons that are variable and analytical in proportions. Noise, interference between adjacent anomalies, extremely large window size of the anomalous data among others is possible factors responsible for the generation of invalid Euler solutions. Several strategies are utilized for the detection and removal of invalid solutions. Isolated solutions (solutions that are greater than certain specified distance from other solutions) are rejected and solutions lying far from the window where the data points producing them are concentrated may also be rejected. A workable approach which provides summarized useful methods was presented by [92].

Furthermore, a different approach can be used to examine how well Euler's equation fits the solution fits the generated solution individually by each data as observed in equation 18.

$$Err_i = \frac{\partial h_i}{\partial p_i}(p_i - p_0) + \frac{\partial h_i}{\partial r_i}(r_i - r_0) + SI.\ h_i \quad (18)$$

where $(p_0,\ r_0)$ is the localized position of Euler solution that were generated from a window of data points centered on $(r_i - r_0)$ where Err_i is the resultant error function. It is worthy of note that the error function is not expected to be zero when calculated at any given point because a window of data points was utilized in the generation of each solution. However, when a large error is encountered, the problems are identified and the solution may consequently be rejected [84]. Though, smaller window sizes can enhance the identified possible solution clustering when permitted by the levels of the prevailing data noise. Also, though the method may not be computer intensive with the time taken being proportional to the number of generated solutions but searching for the isolated solutions by comparatively observing the distance between each solution and every other operation is highly intensive computationally, with the time taken being proportional to the square of the number of generated solutions. It has been proven overtime that the solution rejection techniques are capable and highly effective in retaining solutions that are found as clusters around or near the edges of the causative bodies, and rejecting those that are located far from them or extremely deep to be identified with them [84].

Data Acquisition and Processing.

The aeromagnetic datasets of Ilorin (sheet 223) that were acquired from the Nigerian Geological Survey Agency (NGSA) were prepared with Microsoft Excel program, and processed and interpreted using Oasis Montaj 8.4V. The datasets were imported and transferred to Universal Transverse Mercator (UTM) Zone 31N from UTM Zone 32N in order to maintain a constant coordinate system and to avoid misinterpretation of the acquired data by minimizing distortion over certain areas in the study location as it is found within UTM Zone 31N [93-94]. According to Nigeria Geological Survey Agency [95-96], the acquired datasets were part processed by Fugro Airborne Surveys (Leidschendam, Netherlands) using UTM of Zone 32N (UTM-32N) projection and World Geodetic System, 1984 (WGS84) as the reference datum. The WGS84 is a global datum used for determining position on the earth's surface (Figure 3.10). The WGSS84 has been a reference system harnessed by the satellite navigation system like GPS and consequently utilized in various mapping applications. It is often employed in the determination of varying positions on the earth's surface. The WGSS84 datum is expressly represented and maintained by the United States National Geospatial-Intelligence Agency (US-NGA). Coordinates computed from GPS receivers and are typically provided in terms of the WGS84 datum. WGS84 is highly compatible with the International Terrestrial Reference System (ITRS). De-culturing, tie-line and micro-leveling are some of the pre-processing operations carried out on the data. The datasets were given out by NGSA as an ASCII file comprising of X, Y and Z columns corresponding to the longitudes, latitudes and their matching total magnetic field intensities respectively. The total magnetic field intensity "Z" was stripped of 33,000nT for ease of processing the airborne data [95].

Structural and Geological Limitations of Euler Deconvolution Technique

Despite the widespread application of Euler Deconvolution, it has significant limitations and it is susceptible to errors if integrated without proper caution. Among these limitations are simplistic model assumption; Euler deconvolution assumes simple, isolated and homogeneous sources like prisms, cylinders and contacts. It struggles and negotiates with complex, dipping or non-homogeneous geological bodies. Invalid for deep undulating surfaces; this record may be ineffective for mapping large scale, deep undulating surfaces like the Moho or deep sedimentary basins because these structures do not fit the required simple, homogeneous and isolated edge models. Linear regional issues; if a significant regional gradient is not removed, it can be misinterpreted as a source creating false solutions [93-94]. Also, the generation of spurious solutions could be as a result of misplaced solutions where the algorithm often generates a ray of solution often called Euler tails that are not located over the true source particularly when the

assumed geological model is incorrect. Interference issues may occur when multiple, closely spaced sources exist thereby making Euler deconvolution to create false, scattered solutions in between the actual bodies. Noise sensitivity is another is another critical issue that often produces spurious solutions because the technique involves the calculations of derivatives which amplifies noise and data with low signal to noise ratios often produces erratic, non-physical or scattered outputs [84, 92].

RESULTS AND DISCUSSION

Analytical Signal Map

The analytical signal (AS) map enhances the variations in the magnetization of magnetic sources and highlights peaks of magnetic signatures in the study area. The legend of AS map (Figure 3) reveals a value range of 0.0002 to 3.4127 nT/m with its highest peak (0.2071 to 3.4127 nT/m) mostly concentrated at the NE-SW portions of the area while the lowest peaks (0.0136 to 0.0002nT) could be observed as splashes and dots of splashes concentrated from the NW and distributed across the SE portion trending more prominently to the NS portion of the area. Areas observed to exhibit high values from the Analytical Signal maps suggests that the structural features over those areas are playing host to these shallow sources or the lineaments in the areas were filled with magnetic minerals [92]. Anomaly values that ranged from 0.00 to 0.12 nT/m, with highest peak of 0.02 to 0.12nT/m have been reported in Abeokuta and its environs [93-94]

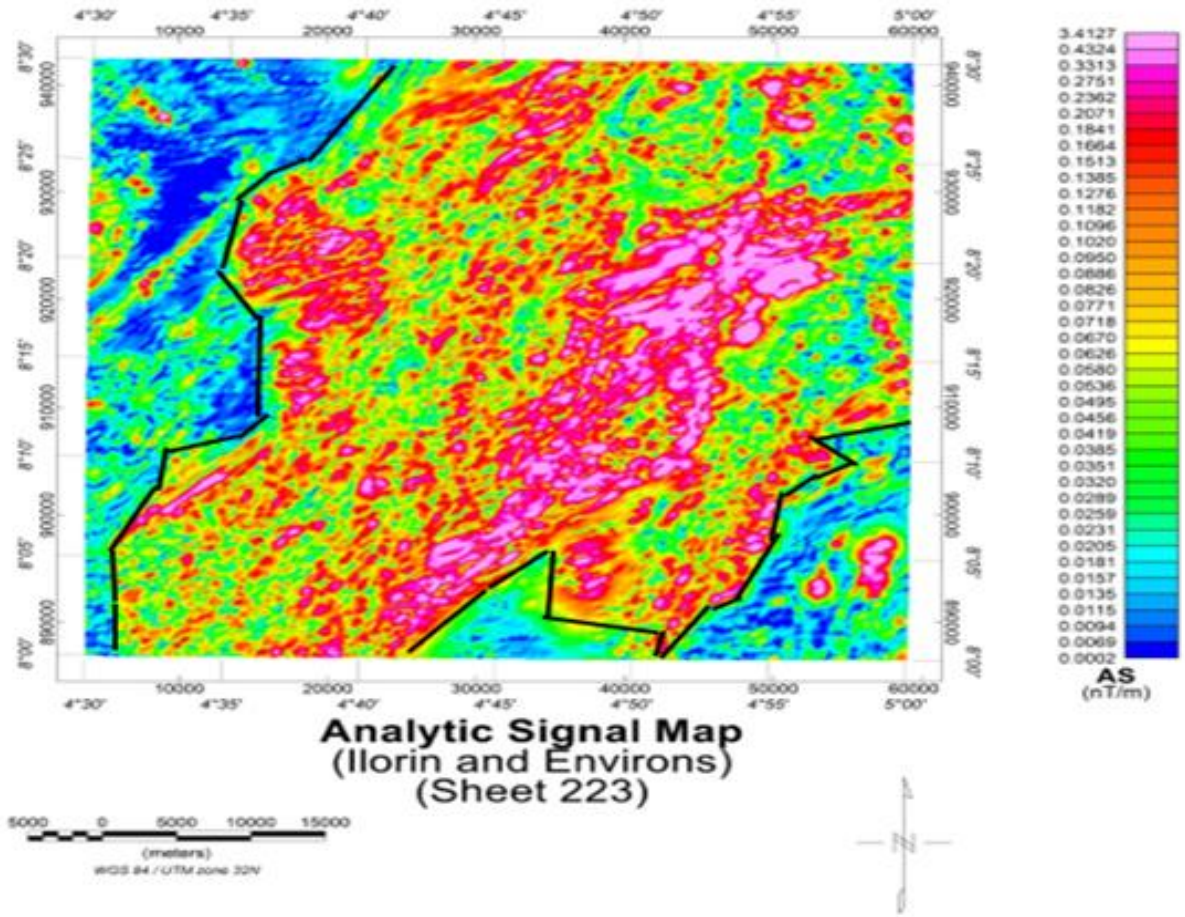

Figure 3: Analytical Signal Map of Ilorin and its environs

3D-Euler Deconvolution Technique

This 3D Euler Deconvolution technique play a crucial role in analyzing magnetic data for the purpose of determining the depth of the interface between sedimentary and basement rocks. The precision of its outcomes is heavily impacted by elements like the structural index, sampling frequency and the quality of the Magnetic data. Additionally, a thorough grasp of the subsurface geological environment is crucial [76-77]. Euler's homogeneity equation which incorporates a base level for the background magnetic field can be represented as follows:

$$(p - p_0)\frac{\partial H}{\partial p} + (q - q_0)\frac{\partial H}{\partial q} + (r - r_0)\frac{\partial H}{\partial r} = N(B - H) \qquad (19)$$

In this context, H represents the total magnetic field observed at the coordinates (p, q, r) with the source located at (p_0, q_0, r_0). B represents the regional or background field while N otherwise termed the structural index indicating the level of uniformity. The structural index measures how quickly the magnetic field diminishes and is closely linked to the shape of the magnetic source [74-76]. The expressed equation above (19), which contains four unknowns p_0, q_0, r_0 and B can be solved through a least square mathematical approach.

In this study, 3D Euler Deconvolution method was used to estimate the depth to the basement of anomalies density present in the study area. The collected datasets were tested for different source geometries i.e., Contacts, thin beds, horizontal cylinders, and spheres which correspond to structural indices of 0, 1 and 2 respectively as captured in structural index for geological model (Table 1). Only the Euler solutions corresponding to source geometry of thin beds (faults/dykes/sills) of S.1=1 in the magnetic column was considered appropriate to be used (Table 1). Therefore, the map (Figure 4) shows the result of Euler Solution for the structural index of 1 which is used to solve for source geometry of a thin bed fault. This solution was considered more appropriate because it contains less spurious solutions after windowing and geologically meaningful interpretations can be deduced from the map. A depth range of 96m to 292m which was considered to be the depth range of near surface contact intrusive rocks was recorded while the maximum depth range of 268m to 292m depicts the location of long wavelength magnetic anomalies. While the entire depth values ranged from 96m to 292m, the patterned continuous elongation of contours and the NNE and SSW parts of the study area conforms to the fault structures interpreted in qualitative analysis and when compared with the geological map of Ilorin and its environs. The light blue/deep blue colourations of the patterned contours interpreted as fault structures shows that they were found to be at shallow depths. The presence of fault/structures serves as conduits or entrapment for solid or ore minerals as well as groundwater accumulation.

Table 1: Structural Index for Geologic Models [65, 74-76]

Geological Model	Number of Infinite Dimension	Gravity S1	Magnetic S1
Sphere	0	2	3
Pipe	1(Z)	1	2
Horizontal Cylinder	1(X or Y)	1	2
Dyke	2(Z and X or Y)	0	1
Sill	2(X and Y)	0	1
Contact	3(X, Y and Z)	0	0

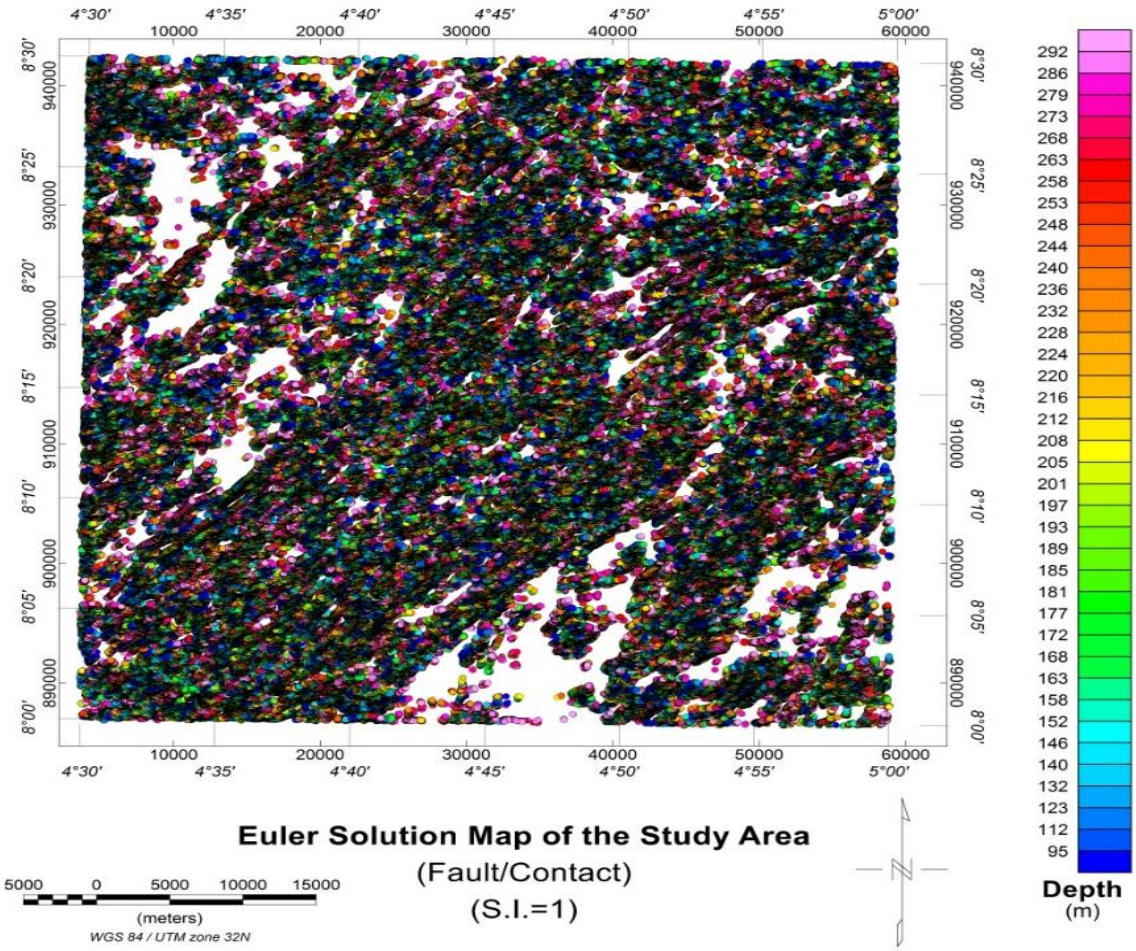

Figure 4: 3D Euler Solution Map (S.I = 1) of Ilorin and its environs

CONCLUSION

This study focuses on using high-resolution aeromagnetic data to investigate subsurface geological structures situated within the schist and Migmatite-Gneiss complex over Ilorin and its environs (sheet 223), North-Central Nigeria. This study has revealed the robustness of a simultaneous Euler deconvolution of both horizontal and vertical gradients with respect to noise. The application of Euler deconvolution to a complex quantity like analytic signal produced superior outputs when compared with those derived from the conventional approach of the deconvolution of the analytic signal amplitude. The techniques for the computation of field gradients in a clean pattern were highlighted alongside with the suggested new technique for rejecting invalid Euler solutions while the modified Euler deconvolution algorithm was equally demonstrated exemplifying it on synthetic models as well as on the high-resolution aeromagnetic data of the study area. Data acquired from the Nigerian Geological Survey Agency (NGSA) were processed using Geosoft Oasis Montaj. Key processing filters (e.g., low-pass Gaussian), and the application of derivative techniques to highlight geological structures such as faults and lithological boundaries. Euler Deconvolution was used as a quantitative measure to estimate the depths and dimensions of magnetic sources. The application of Euler deconvolution to a complex quantity like analytic signal produced superior outputs when compared with those derived from the conventional approach of the deconvolution of the analytic signal amplitude. Structural trends mainly aligned NNW–SSE and NE–SW, consistent with known tectonic features from the Pan-African Orogeny. This study has enhanced the understanding of Ilorin's geology using high-

resolution aeromagnetic data. The analytical signal revealed a value range of 0.0002 to 3.4127 nT/m while the 3D Euler Deconvolution revealed a depth value ranging from 95m to 292m; estimating the depth and geometry of magnetic sources. The integration of quantitative results indicates that the area is structurally complex, with multiple fractures, faults and lithological boundaries concealed beneath the surface. The analysis revealed variations in magnetic intensity linked to different rock types and degrees of metamorphism within the basement complex. Depth estimates from Euler deconvolution showed both shallow and deep magnetic sources. Overall, the study revealed significant structural features that can guide further geological, mineral and hydrogeological exploration in the area. The structurally controlled and anomalous zones identified should be considered for future mineral exploration due to their potential economic value. These features serve as potential targets for mineral deposits, groundwater accumulation, and geotechnical assessments. This study has demonstrated the effectiveness of aeromagnetic techniques in unraveling subsurface geology and supports informed resource management in Ilorin and its environs. Findings from this study can also support informed decisions in urban development and infrastructure planning across Ilorin and its environs.

REFERENCES

[1] Keating, P. (1995). A simple technique to identify magnetic anomalies due to Kimberlie pipes: exploration. Mining Geology; 4(1): pp. 121-125.

[2] Pier, M., Belcourt, G., and Rockel, E. (2000). Geophysical methods for Kimberlite exploration in Northern Canada. The Leading Edge; 23(1): pp. 11-24. https://doi.org.10.1190/1825939

[3] Gulmanias, J., Batchelor, T., Doe, S and Pascual-Cebirian, E. (2015). Hydrocarbon production from fractured basement reservoirs. https://www.geoscience.co.uk/technical.pipes

[4] Smith, D.V., and Pratt, D. (2003). Advanced processing and interpretation of the high resolution aeromagnetic survey data over the central aquifer, Texas: Proceedings from the symposium on the application of Geophysics to Engineering and Environmental Problems. Environmental and Engineering Society. https://doi.org.10.4133/1.2923181

[5] Timur, E. (2017). Assessment of vertical magnetic gradient data of Tuzla fault using boundary analysis and 3D inversion techniques. Journal of Power and Energy Engineering; 5(12): pp. 33-45. https://doi.org.10.423611pec.2017.512006

[6] Tsokas, G.N and Papazachos, C.B (1992). Two-dimensional inversion fitters in magnetic prospecting: Application to the exploration for buried antiquities. Geophysics; 57(1): pp. 1004- 1013. https://doi.org.10.1190/1825939

[7] Timur, E. (2014). Magnetic susceptibility and VLF-R investigations for determining geothermal blowout contaminated area: a case study from Alasehir (Menisa/Turkey). Environmental Earth Sciences. 72(1): pp. 2497-2510. https://doi.org.10.1007/s12665-014-3158-0

[8] Smith, R.P., Grauch, V.J.S., and Blackwell, D.D. (2002). Preliminary results of a high resolution aeromagnetic survey to identify buried faults at Dixie valley. Nevada. Geothermal Resources Council Transactions; 26(1): pp. 543-546.

[9] Goussev, S.A., Griffith, L., Pierce, J and Cordsen, A. (2004). Enhanced HRAM anomalies correlate faults between 2D seismic lines. *74th Annual International Meetings, SEG Extended Abstract.* 730.

[10] Grauch, V.J.S., Hudson, M.R., and Minor, S.A. (2001). Aeromagnetic expression of faults that offset basin fill, Albuquerue basin, New Mexico. Geophysics; 66(1): pp. 707-720.

[11] Pierce, J.W., Goussev, S.A., Mchean, R., and Menshal, M. (1999). Aeromagnetic interpretation of the Dianango trough HRAM survey, onshore Gabon. *69th Annual International Meeting,* SEG Extended Abstract; pp. 343-346.

[12] Prieto and Morton, 2003; Prieto, C and Morton, G. (2003). New insights from a 3D Earth Model, Deepwater Gulf of Mexico. The leading Edge; 22(1): pp. 356-360. https://doi.org.10.1190/1.1572090

[13] Ross, G.M., Broome, J and Miles, W. (1994). Potential fields and basement structure. Western Canada Sedimentary Basin. In Morsop, G.D and Shetsen, J. Eds, Geological Atlas of the Western Canada Sedimentary Basin. Canadian Society of Petroleum Geologists and Alberta Research Council; pp. 41-46.

[14] Nabighian, M.N., and Hansen, R.O. (2001). Unification of Euler and Werner deconvolution in three dimensions via the generalized Hilbert Transform. Geophysics; 66(1): pp. 1805-1810.

[15] Nabighian, M.N., Grauch, V.J.S., Hansen, R.O., Lafehr, T.R., Li, Y., Pierce, J.W., Phillips, J.D and Rander, M.E. (2005). The historical development of the magnetic method in exploration geophysics. Geophysics; 70(6): pp. 33-61. https://doi.org.10.1190/1.21337841

[16] Salawu, N.B., Olatunji, S., Adebiyi, L.S., Olasunkanmi, N.K and Dada, S.S. (2019). Edge detection and magnetic basement depth of Danko area. Northwestern Nigeria from low-latitude aeromagnetic anomaly data. SN Applied Sciences; 1(1056): pp. 1-8.

[17] Murthy, I.V.R. (1990). Magnetic anomalies of industrial pipes and algorithm for magnetic inversion of dykes and basement topographies. Proceedings of Indian Academy of Sciences*;* 99(1): pp. 549-579.

[18] Murthy, I.V.R. (1998). Gravity and magnetic interpretation in exploration geophysics. Geological Society of India. Bangalore, Geological Society of India Journal; pp. 363.

[19] Murthy, I.V.R. and Krishnamacharyulu, SK.G (1990). Automatic inversion of gravity anomalies of faults. Computers and Geosciences; 16(1): pp. 539-548. https://doi.org.10.1016/0098-3004(90)90014-k

[20] Rao, D.B. and Babu, N.R. (1993). A fortran-77 computer program for 3 dimensional inversion of magnetic anomalies resistivity from multiple prismatic bodies. Computers and Geosciences; 19(1): pp. 781-801. https://doi.org.10.1016/0098-3004(93)90050-F

[21] Dara, O., Candan, O., Dur, S and Oberhansil, R. (1997). New evidence on the geotectonic evolution of the Menderenes Massif. In Piskin,O., Savasien, M.Y., Ergwu, M and Tarcan, G. Eds. Proceedings International Earth Sciences Colloquium on the Aegean Region; 19951(10): pp. 53-72.

[22] Genc, S.C., Altankaynak, S., Yazman, M and Yilmaz, Y. (2001). The Cubuklu-dug graben, Smith of Izmir: its tectonic significance in the Neogene geological evolution of the Western Anatola. Geodinamica Acta; 14(1): pp. 45-55. https://doi.org.10.1016/50985-3111(00)01061-5

[23] Roest, W.R., Verhoef, J and Pilkington, M. (1992). Magnetic interpretation using the 3D Analytic Signal. Geophysics; 55(1): pp. 116-125. https://doi.org.10.1190/1.1443174

[24] Arisoy, M.O and Ulugergerli, E.U. (2005). Evaluation of different receiver orientations and receiver separations in magnetic groundwater method. Journal of Balka Geophysical Society; 8(1): pp. 229-232.

[25] Blakely, R.J. (1995). Potential theory in gravity and magnetic applications. Cambridge University Press. https://doi.org.10.1017/CNO9780511549816

[26] Ekwok, S.E., Akpan, A.E., Ebong, E.D., and Eze, O.E. (2021). Assessment of depth to magnetic sources using high resolution aeromagnetic data at some parts of lower Benue trough and adjoining areas, Southeast Nigeria. Advances in Space Research; 67(3/4): 11-21. https://doi.org.10.1016/j.asr.2021.01.007

[27] Hsu, S.K. (2002). Imaging magnetic sources using Euler's equation. Geophysical Prospecting; 50(1): 15-25.

[28] El-Dawn, M.G., Tianyouw, L., Hui, S., and Dopeng, L. (2004). Depth estimation of 2D magnetic anomaly sources by using euler d3convolution method. American Journal of Applied Science; 1(3): pp. 209-214. https://doi.org.10.3844/ajassp.2004.209.214

[29] Hinze, W.J., Von, F., Ralph, R.B., Saad, A.H. (2013). Gravity and Magnetic Exploration principles, practices and applications. Cambridge University Press. pp. 23-27.

[30] Abubakar, I., Borde, D.S., and Raboh, Y. (2019). Basement depth estimation usingEuler Deconvolution and source parameter imaging: a case study of Northwestern part of Sokoto Basin. Saudi Journal of Engineering and Technology; 4(9): pp. 387-392.

[31] El-Bohoty, M., Khalil, A., Hussain, W., El-kotb, A., Awad, A., and Khalifa, M. (2021). Geophysical studies of subsurface structures of the area surrounding the new part of Jarjob in El-Negila-Massa Matruh using magnetic data. NRIAG Journal of Astronomy and Geophysics; 10(1): pp. 456-471. https://doi.org.10.1080/20900977.2021.1907963

[32] Keating, P and Pilkington, M. (2004). Euler deconvolution of the analytic signal and its application to magnetic interpretation. Geophysical Prospecting; 52(3): pp. 165-182. https://doi.org.10.1111/j.1365-2478-2004.00408.x

[33] Yandjimain, J., Ndougsa-Mbargo, T., Bi-Alow, M.B., and Meying, A. (2018). Aeromagnetic data modeling for geological and structural mappings over the DJADOM-ETA area in the southeastern Cameroon. International Journal of Geosciences; 9(6): pp. 54-59. https://doi.org.10.4236/ijg.2018.96022

[34] Abubakar, F., Fatoye, F.B., Abdulsalami, M.J., and Aliyu, A. (2025). Aeromagnetic delineation of Iron ore deposits in a complex geological terrain aided by fuzzy logic. Geodynamic and Geoenvironment; 4(4): pp. 455-453. https://doi.org.10.1016/geogeo.2025.100410

[35] Megawara, T., and Udensi, E.E (2014). Structural analysis using aeromagnetic data: case study of parts of Southern Bida Basin, Nigeria and the surrounding basement rocks. Earth Science Research; 3(2): pp. 10-13. https://doi.org.10.5539/esr.v3n2p27

[36] Martins, O.E., Mosto, O.K., and Ifeanyi, O.A. (2021). Aeromagnetic interpretation of basement structure and architecture of the Dahomey basin, Southwestern Nigeria. *NRIAG* Journal of Astronomy and Geophysics; 10(1): pp. 93-109. https://doi.org.10.1080/2099977.2021.1880817

[37] Alao, K., Olagoke, P.O., Suleman, K.O., and Sunmonu, L.A (2024). Determination of depth to magnetic sources using source parameter imaging of high resolution aeromagnetic data of ESIC, North Central Nigeria: an investigation tool for geothermal exploration. International Journal; 4(6): pp. 1091-1094. https://doi.org.10.62225/2583049x.2024.4.6.3559

[38] Ekwok, S.E., Achadu, O.M., Akpan, A.E., Eldosouky, A.M., Ufuafuonye, C.H., Abdelrahman, K., and Gomez-Ortiz, D. (2022). Depth estimation and basement rocks in the Bornu Basin, North-West Nigeria using High Resolution Airborne Magnetic Data. MDDP Minerals; 12(3): pp. 445-462. https://doi.org.10.3390/min12030285285

[39] Hakeem, B.O., Saminu, O., Abdulgafar, J., and Haydar, A. (2021). Aeromagnetic and resistivity technique for investigating leakage parts in Apsdu Dam Ilorin, Sheet 201. South-West Nigeria. The NEXUS Science Edition; 1(1): pp. 12-21.

[40] Fatoye, O.V., Adebayo, S.A., Ayeni, J.K., and Ibiwoye, J.O. (2025). Subsurface geology and structural trend evaluation of dam using multi-techniques. Discover Geosciences; 3(39): pp. 101-107.

[41] Olanrewaju, T., Salawu, T.O and Orosun, M.M. (2016). Application of 3D-Euler deconvolution technique to aeromagnetic data of Ilorin and Osi, Northern Nigeria. Zambian Journal of Science and Technology; 11(1): pp. 66-75.

[42] Salem, A., Williams, S., Fairhead, D., Smith, R and Ravat, D. (2008). Interpretation of magnetic data using tilt angle derivatives. Geophysics; 73(1): pp. 1-10

[43] Saada, S.A. (2016). Curie point depth and heat flow from spectra analysis of new magnetic data over the Northern part of Western Desert, Egypt. Journal of Applied Geophysics; 134(1): pp. 100-111. https://doi.org.10.1016/j.jappgeo.2016.09.003

[44] Phillips, J.D. (2000). Locating magnetic contacts: a comparison of the horizontal gradient, analytical signal and local wave number methods. In SEG Technical Programme Expanded Abstracts 2000; pp. 402-405.

[45] Verduzco, R., Fairhead, J.D., Green, C.M., and Mackenzie, C. (2004). New insights into the magnetic derivatives for structural mapping. Leading Edge; 23(10): pp. 116-119.

[46] Muzaffer, O.A., and Unal, O. (2013). Edge detection of magnetic sources using enhanced total horizontal derivative of the tilt angle. Yerbilimleri; 34(1): pp. 73-82.

[47] Sherrif, S.D. (2010). Matched filter separation of magnetic anomalies caused by scattered surface debris at archaeological sites. Near Surface Geophysics; 8(1): pp. 145-150.

[48] Agoha, C.C., Onwubuariri, C.N., Mgbeojedo, T.I., Amasike, C.U., Agbakwuru, C.B., Njoku, J.O., Akaolisa, C.C.Z., Alexander, O.I., Ofoh, I. (2023). Aeromagnetic Data Integration and Source Body Evaluation using Standard Euler deconvolution Technique in Obudu Area, Southeastern Nigeria. Petroleum and Coal; 65(4): pp. 1033-1041.

[49] Aktas, G. (2024). Edge Detection and Depth Estimation of Lake Sapanca, Eastern Marmara Region from High-Resolution Magnetic Data. Acta Geophysica (Applied Geophysics). 72(1): 3337-3354. https://doi.org.10.1007/s11600-023-01277-0

[50] Reeves, C. V. (2005). Aeromagnetic Surveys, Principles, Practice and Interpretation; Geosoft: 155.

[51] Anthony, E.A., Likkasson, O.K., Maigari, A.S., Ali, S and Abubakar, A. (2023). Subsurface Structural Characterization as deduced from High Resolution Aeromagnetic Data over the Confluence Zones in Central Nigeria. Indonesian Journal of Earth Sciences. 3(1): 322-343. https://doi.org.10.52562/injoes.2023.600

[52] Oruc, B. (2011). Edge detection and depth estimation using a tilt angle map from gravity gradient data of the Kozaklo-central Anatolia Region, Turkey. Pure and Applied Geophysics; 118(10): PP. 69-80. https://doi.org/10.1007/s00024-010-0211-0

[53] Holden, E.J., Fu, S., and Kovesi, P. (2011). Automatic identification of responses from porphyry intrusive systems within magnetic data using image analysis. Journal of Applied Geophysics; 74(4): pp. 255-262.

[54] Ozebo, V.C., Ogunkoya, C.O., Makinde, V., and Omoeke, M.O. (2015). An estimation of magnetic contact location and depth of magnetic sources in Ilesha, Nigeria using magnetic gradient techniques. African Review of Physics; 10(1): pp. 17-26.

[55] Ayomide, A., Felix., O.O., Adeboye, M.B. (2025). Deformation of Depth to Magnetic Sources from Aeromagnetic Data of Idah, Kogi State using Eulr Deconvolution Technique. International Journal of Earth Sciences, Knowledge and Applications; 7(2): pp. 18

[56] Lawal, T.O., Salawu, N.B., Orosun, M.M., Ekpumoh, J.I., Nwankwo, L.I (2016). Application of 3D-Euler deconvolution technique to aeromagnetic data of Ilorin and Oso, North-central Nigeria, Zimbabwe Journal of Science and Technology; 11910: pp. 66-67.

[57] Lawal, T.O., and Nwankwo, L.I (2017). Evaluation of depth to the bottom of magnetic sources and heat flow from high reasolution aeromagnetic data part of Nigerian sector of Chad Basin. Arabian Journal of Geophysics; 1-12. https://doi.org.10.1007/512517-017-3154-2

[58] Awoyemi, M.O., Hammed, O.S., Arogundade, A.B., Ajana, O.D and Iwalehin, P.O (2018). Geophysical investigation of the possible extension of Ifewara fault zone beyond Ilesa area, Southwestern Nigeria. *Arabian Journal of Geosciences;* 10(2): pp. 27. https://doi.org.10.1007/517-016-2813-2

[59] Elkhateeb, S.O and Abdellatif, M.A.G. (2018). Delineation potential gold mineralization

zones in a part of central eastern desert, Egypt using airborne magnetic and radiometric data. NRIAG Journal of Astronomy and Geophysics; 7(2): pp. 361-376. https://doi.org.10.1016/j.nrjag.2018.05.0

[60] Babylon, O.B. (2019). Tectonic and structural analysis of the migmatitic gneiss-quartzite complex of Ilorin area from aeromagnetic data. NRIAG Journal of Astronomy and Geophysics; 8(1): pp. 22-23. https://doi.org.10.1080/20909977.2019.1615795

[61] Wang, Y., Duan, X., and Wang, L. (2019). Spatial distribution and source analysis of heavy metals in soils influenced by industrial enterprise distribution: a case study in Jiangsu Province. Science of Total Environment; 2411-2425 www.sciencedirect.com/science/article/pui/50048969719349459

[62] Lawal, T.O. (2020). Integrated aeromagnetic and aeroradiometric data for delineating lithologies, structures and hydrothermal alteration zones in parts of Southwestern Nigeria. Arabian Journal of Geophysics; 13(775): pp. 1-19. https://doi.org.10.1007/512517-020-05743-7

[63] Lawal, T.O., Sunday, J., Fawale, K., Salami, M., and Adewumi, T. (2021). Use of magnetic anomaly data to delineate subsurface structures and depth characterization of Lafiagi and its environs, North Central Nigeria. NRIAG Journal of Astronomy and Geophysics; 10(1): pp. 155-167. https://doi.org.10.1080/20909977.2021.1900526

[64] Ljhoul, M., Abd-Elhamid, H.F., Abdelrahman, M., Fnais, M.S and Sbistin, K. (2023). Application of enhanced methods of gravity data analysis for mapping the subsurface structure of the Bahira Basin in Morocco. Frontiers Earth Sciences: Security, Environmental Informatics and Remote Sensing. 11(1): pp. 273-279. https://doi.org.10.3389/feart20231225714

[65] Ekwok, S.E., Eldosouky, A.M., Thompson, E.A., Ojong, R.A., George, A.M., Alarifi, S.S., Kharbush, S., Andras, P and Akpan, A.E. (2024). Mapping of geological structures and sediment thickness from analysis of aeromagnetic data over the Obudu basement complex of Nigeria. Journal of Geophysics and Engineering; 21(2): pp. 413-425. https://doi.org.10.1016/geogeo.2025.100410

[66] Abolarin, A. T., and Ibrahim, S. (2015). Evaluation of groundwater occurrences in the Precambrian Basement Complex of Ilorin metropolis, Southwestern Nigeria. RMZ–Materials and Geoenvironment; 62(1): pp. 117-132.

[67] Olabode, S. O., Ajayi, K. T., and Olatunji, M. A. (2014). Structural interpretation of basement terrain using aeromagnetic data. Nigerian Journal of Geosciences*;* 12(1): 45-58.

[68] Olasehinde, P. I., Mohammed, A. A., and Yusuf, T. A. (2020). Groundwater prospecting in crystalline rocks using integrated geophysical methods. Journal of Applied Geophysics; 38(2): pp. 112-124. https://doi.org/10.1234/jag.2020.5678

[69] Njoku, J. O., Nwankwo, L. I., and Uche, E. I. (2022). Aeromagnetic evaluation of crustal structures in north-central Nigeria. International Journal of Earth Sciences; 76(4): pp. 210-225.

[70] Raji, W. O., and Abdulkadir, K. A. (2020). Evaluation of groundwater potential of bedrock aquifers in Geological Sheet 223 Ilorin, Nigeria, using geo-electric sounding. Applied Water Science; 10(1): pp. 220. https://doi.org/10.1007/s13201-020-01303-2

[71] Annor, A. E., Olasehinde P. I. (1996). Vegetation Niche as a Remote Sensor for Subsurface Aquifer: A Geological-Geophysical Study in Jere Area, Central Nigeria. Water Resources Journal of National Association of Hydrogeology; 7(1&2): pp. 26-30.

[72] Offodile, M. E. (1987). An Approach to Groundwater Study and Development in Nigeria. Published by Mecon Services Ltd, Jos, Nigeria. pp. 5-7.

[73] Mushayandebvu, M.F., Van-driel, P., Reid, A.B., and Fairhead, J.D. (2001). Magnetic source parameters of two-dimensional structures using extended Euler deconvolution. Geophysics; 66(1): pp. 814-823.

[74] Ishola, S.A and Olorunnusi, B.A. (2025). Geological and Structural Evaluation using High Resolution Aeromagnetic Data of Ilorin (Sheet 223), North-Central Nigeria. *Unpublished B.sc Degree Project.* 17.

[75] Hartman, R.R., Teskey, D.J., and Friedberg, J.L. (1971). A system of rapid digital aeromagnetic interpretation. Geophysics; 36(1): pp. 891-918.

[76] Thompson, D. T. (1982). EULDPTH: A new technique for making computer-assisted depth estimates from magnetic data: Geophysics; 47: pp. 31–37.

[77] Reid, A. B., Allsop J. M., Granser H., Millett A. J., Somerton I. W. (1990). Magnetic interpretation in three dimensions using Euler Deconvolution. Geophysics; 55: pp. 80–91. https://doi.org.10.1190/1.1442774

[78] Cooper, G.R.J. (2004). Euler deconvolution applied to potential field gradients. *Exploration Geophysics.* 35(1): 165-170.

[79] Marson, J and Kingele, E.E. (1993). Advantages of using vertical gradient of gravity for 3D interpretation. Geophysics; 58(1): pp. 1588-1595.

[80] Stavrev, P.Y. (1997). Euler deconvolution using differential similarity transformation of gravity or magnetic anomalies. Geophysical Prospecting; 45(1): pp. 207-246.

[81] Ravat, D., Kirkham, K, and Hildenbrand, T.G. (2002). A source depth separation filter using the Euler method on the derivatives of total intensity magnetic anomaly data. The Leading Edge; 21(1): pp. 360-365.

[82] Cooper, G.R.J and Crown, D.R. (2002). Applications of fractional calculus to potential field data. Exploration Geophysics; 34(1): pp. 51-56.

[83] Cooper, G.R.J. (2002). An improved Algorithm to the Euler deconvoluion of potential field data. The Leading Edge; 21(1): 1197-1198.

[84] Huang, D., Gubbins, D., Clark, R.A., and Whaler, K.A. (1995). Combined study of Euler's homogeneity equation for gravity and magnetic field: 57th EAGE Conference and Technical Exhibition. Abstract; pp. 11-17.

[85] Zhang, C., Mushayandebvu, M.F., Van-Driel, P., Reid, A.B., Fairhead, J.D., and Odegard, M.E. (2000). Euler deconvolution of gravity tensor gradient data. Geophysics; 65(1): pp. 512-520.

[86] Salem, A and Ravat, D. (2003). A combined analytic signal and Euler method (ANA-EUL) for the automatic interpretation of magnetic data. Geophysics; 68(1): pp. 1952-1961.

[87] Ghosh, G.K., Gupta, R.D., Khanna, A.K., and Singh, S.N. (2012). Application of Euler Deconvolution of Gravity and Magnetic Data for Basement Depth Estimation in Muzoram Area. Geohorizons; 1(3): pp. 25-30.

[88] Malleswara-Rao, M.M., Lakshminarayana, S., Murthy, K.S.R and Subrahmanyam, A.S. (1993). Two ComputerPrograms for the Analysis of Marine Magnetic Data. Computer and Geosciences; 19(5): pp. 657-672.

[89] Thurston, J. B., Smith, R. S., (1997). Automatic conversion of magnetic data to depth, dip and density contrast using the SPI method. Geophysics; 62 (3): pp. 807–813.

[90] Melo, F.F., Barbosa, V.C.F., Uieda, L., Oliviera, V.C., Silver, J.B.C. (2013). Estimating the Nature and the Horizontal and Vertical Positions of the 3D Magnetic Sources using Euler Deconvolution. Geophysics; 78(6): pp. 187-198. https://doi.org.10.1190/geo2012-0515.1

[91] Fedi, M and Florio, G. (2001). Detection of potential field source boundaries by enhanced horizontal derivative method. Geophysical Prospecting; 49(1): pp. 40-58.

[92] FitzGerald, D., Reid, A.B., and Mclnerney, P. (2004). New discrimination techniques for Euler deconvolution. Computer and Geosciences; 30(1): pp. 461-469.

[93] Chukwu, C., Betts, P., Moore, D., Munukutia, R., Armigt, R., McLean, M., and Grose, L. (2023). Unsupervised machine learning and depth clusters of Euler deconvolution to magnetic data: a new approach to imaging geological structures. Exploration Geophysics. 55(3): pp. 451-462. https://doi.org/10.1080/08123985.2023.2299475

[93] Hosseni, S.H., Afshar, A., Adedi, M., Ganbarifar, S., Oskodi, B., and Moradi, S. (2025). Fixed window joint Euler deconvolution for depth estimation of magnetic and gravity data in the Scavaz region. Scientific Reports. 15(3): pp. 41-55. https://doi.org/10.1038/s41598-025-2620-9